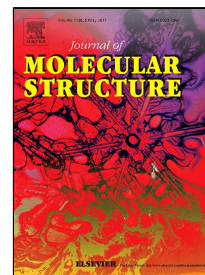


Accepted Manuscript

Spectroscopic, DNA Binding Ability, Biological, DFT Calculations, and Non Linear Optical Properties (NLO) of Novel Co(II), Cu(II), Zn(II), Cd(II) and Hg(II) Complexes with ONS Schiff base



Ayman A. Abdel Aziz, Fatma M. Elantabli, H. Moustafa, Samir M. El-Medani

PII: S0022-2860(17)30369-1
DOI: 10.1016/j.molstruc.2017.03.081
Reference: MOLSTR 23577
To appear in: *Journal of Molecular Structure*
Received Date: 03 January 2017
Revised Date: 02 March 2017
Accepted Date: 20 March 2017

Please cite this article as: Ayman A. Abdel Aziz, Fatma M. Elantabli, H. Moustafa, Samir M. El-Medani, Spectroscopic, DNA Binding Ability, Biological, DFT Calculations, and Non Linear Optical Properties (NLO) of Novel Co(II), Cu(II), Zn(II), Cd(II) and Hg(II) Complexes with ONS Schiff base, *Journal of Molecular Structure* (2017), doi: 10.1016/j.molstruc.2017.03.081

This is a PDF file of an unedited manuscript that has been accepted for publication. As a service to our customers we are providing this early version of the manuscript. The manuscript will undergo copyediting, typesetting, and review of the resulting proof before it is published in its final form. Please note that during the production process errors may be discovered which could affect the content, and all legal disclaimers that apply to the journal pertain.

High light (for review)

- Spectroscopic characterization of synthesized ligand and its complexes.
- UV-Vis spectroscopy and fluorescence studies suggest the binding of complexes to DNA.
- The complexes have antimicrobial activities and high thermal stability.
- The HOMO and LUMO energies were computed and discussed.
- The NLO parameters of the complexes show promising optical properties.

Spectroscopic, DNA Binding Ability, Biological, DFT Calculations, and Non Linear Optical Properties (NLO) of Novel Co(II), Cu(II), Zn(II), Cd(II) and Hg(II) Complexes with ONS Schiff base

Ayman A. Abdel Aziz^a, Fatma M. Elantabli^b, H. Moustafa^c and Samir M. El-Medani^{b,*}

^a Department of Chemistry, Faculty of Science, Ain Shams University, Cairo 11566, Egypt.

^b Department of Chemistry, Faculty of Science, Fayoum University, El-Fayoum, Egypt.

^c Department of Chemistry, Faculty of Science, Cairo University, Giza, Egypt.

Abstract

The reaction of Co(II), Cu(II), Zn(II), Cd(II) and Hg(II) with the synthesized N-(2-hydroxy-1-naphthylidene)-2-aminothiophenol Schiff base ligand (H₂L) at room temperature resulted in the formation of the five complexes; [Co(HL)₂]H₂O, **1**; [M(HL)₂] (M= Cu, Zn and Cd), (**2-4**) and [Hg(HL)Cl], **5**. The ligand and its complexes were characterized based on elemental analyses, IR, ¹H NMR, magnetic measurement, molar conductance, and thermal analysis. Coats and Redfern method was used to compute the kinetic and thermodynamic parameters. Antibacterial activities of H₂L and its complexes have been studied. The binding of Co(II), Cu(II) and Zn(II) complexes to calf thymus DNA (CT-DNA) has been investigated using UV-Vis and fluorescence absorption spectra. The results indicated that the ligand and its complexes may bind to DNA by intercalation modes, with a much higher binding affinity of the complexes than that of the ligand. The equilibrium geometries of the studied complexes are investigated theoretically at the B3LYP/LANL2DZ level of theory, and it was found that these geometries are non-linear. The calculated E_{HOMO} and E_{LUMO} energies of the studied complexes can be used to calculate the global properties. The calculated nonlinear optical parameters (NLO); first order hyperpolarizability (β) of the studied complexes show promising optical properties.

Keywords: Asymmetric Schiff base; Metal complexes; DNA-binding studies; DFT calculations; NLO properties.

*Corresponding Author: Professor Dr. Samir M. El-Medani, Department of Chemistry, Faculty of Science, Fayoum University, El-Fayoum, Egypt.
E-mail address: samirmedani20@gmail.com.

1. Introduction

Schiff bases have a great interest for their important properties, such as their catalytic activity in the hydrogenation of olefins [1], ability to reversibly bind oxygen in epoxidation reactions [2, 3], photochromic properties [4, 5] and complexing ability towards some toxic metals [6]. Moreover, Schiff base complexes displayed an important role in biological activity applications [7-10].

Many investigations have been widely studied on metal complexes of Schiff bases containing N and/or O donor sites, [11-15], while fewer studies were performed for those having an ONS donor atoms [16-18]. For example, complexes of salicylideneimine-2-thiophenol with some divalent ions such as Co(II), Ni(II), Cu(II), Zn(II) and Ru(II) were investigated [19, 20]. Furthermore, the structures of ruthenium and osmium carbonyl complexes were investigated and suggested the coordination of metals to salicylideneimine-2-thiophenol ligand via S and N atoms leaving the OH group free [21].

In the literature, there is no systematic study of the electronic structure and nonlinear properties of the studied complexes. Such study is important for understanding the biological activity and NLO properties of these complexes. Non-linear optical properties (NLO) are the ability of any compound to convert light [with intense electric field (LASER)] of longer wave length into light of shorter wave length.

An interesting analytical application of N-(2-hydroxy-1-naphthylidene)-2-aminothiophenol Schiff base had been previously studied by our research group [22], and in view of the diversified roles of Schiff base metal complexes, in the present work, Co(II), Cu(II), Zn(II), Cd(II) and Hg(II) complexes were synthesized and fully characterized by different spectroscopic methods. The antibacterial and antifungal activities of the ligand and the complexes were performed. Furthermore, DNA binding interaction with calf-thymus DNA (CT-DNA) have been elucidated by electronic absorption spectral titration and steady state fluorescence competition studies. The geometrical parameters and NBO analysis are also calculated using B3LYP/LANL2DZ. The first order hyperpolarizability (β) values of the studied complexes has been computed to study the NLO properties. Finally, global reactivity descriptors including electronegativity (χ), hardness (η), softness (S) of the studied complexes were calculated and analyzed.

2. Experimental

2.1. Reagents

The metal salts $\text{Co}(\text{NO}_3)_2 \cdot 6\text{H}_2\text{O}$, $\text{Cu}(\text{NO}_3)_2 \cdot 2.5\text{H}_2\text{O}$, $\text{Zn}(\text{NO}_3)_2 \cdot 6\text{H}_2\text{O}$, CdSO_4 , HgCl_2 , 2-hydroxy-1-naphthaldehyde and 2-aminothiophenol were purchased from Aldrich. All chemicals and solvents were of analytical reagent grade and they were used without further purification.

2.2. Instrumentation

Infrared measurements were carried out on a Unicam-Mattson 1000 FT-IR spectrometer using KBr discs. Electronic absorption spectra were measured on a Unicam UV2-300 UV-VIS spectrometer. Nuclear magnetic resonance measurements were performed on a Spectrospin-Bruker AC 200 MHz spectrometer. Samples were dissolved in $\text{DMSO-}d_6$ using tetramethylsilane as internal reference. Magnetic susceptibilities of the complexes in the solid state (Gouy method) were recorded on a Sherwood Scientific magnetic susceptibility balance. Elemental analyses were performed on a Perkin-Elmer 2400 CHN elemental analyzer. Mass spectra of the solid complexes (70 eV, EI) were carried out on a Finnigan MAT SSQ 7000 spectrometer. Measurements of the thermogravimetric analysis TGA and DTG were carried out under nitrogen atmosphere with a heating rate of $10\text{ }^\circ\text{C}/\text{min}$ using a Shimadzu DT-50 thermal. Electronic spectra were recorded on Shimadzu UV-Vis 1800 spectrophotometer. Fluorescence measurements were carried out on a Jenway 6270 Fluorimeter. The excitation source was a Pulsed Xenon Lamp. All conductivity measurements were performed in DMF ($1 \times 10^{-3}\text{ M}$) at $25\text{ }^\circ\text{C}$, by using Jenway 4010 conductivity meter.

2.3. Synthesis of *N*-(2-hydroxynaphthylidene)-2-aminothiophenol Schiff base (H_2L)

The ligand H_2L (**Scheme 1**) was synthesized as reported in literature [23] by refluxing a mixture of (10 mmol, 1.72 g) of 2-hydroxynaphthaldehyde and (10 mmol, 1.1 mL) of 2-aminothiophenol in about 30 ml absolute ethanol. The reaction mixture was heated to reflux for 2 hours. The reaction mixture was left to cool at room temperature. The solid yellow product was separated and crystallized from hot ethanol and dried on vacuum line to give yellow crystals of the Schiff base ligand (yield 90%). TLC checked the purity of the ligand.

2.4. Synthesis of metal complexes

All complexes were prepared according to the following general procedure. Aqueous solution of the metal salt (1mmol, 10 mL) was added dropwise to an ethanolic solution of H_2L ligand (1mmol, 0.279 g, 25 mL) at room temperature with constant stirring for 10 minutes. The

produced precipitate was isolated by filtration, then washed several times with 3:1 ethanol-water mixture followed by ether.

2.5. Antimicrobial activity

2.5.1 Bacterial susceptibility screening

In vitro antibacterial activity of synthesized compounds was studied against Gram- positive and Gram- negative bacteria by the agar well diffusion [24]. Mueller Hinton agar was used as the bacteriological medium. The compounds were dissolved in 10% aqueous dimethylsulfoxide (DMSO) to a final concentration of 100 µg/100 µL. Pure DMSO was taken as the negative control and 100 µg/100 µL Streptomycin as the positive control. 100 µL of inoculum was aseptically introduced onto the surface of sterile agar plates and sterilized cotton swabs were used for the even distribution of the inoculum. Wells were prepared in the agar plates using a sterile cork borer of 6.0 mm diameter. 100 µL of the test and control compound were introduced in the well. The same procedure was used for all the strains. The plates were kept in laminar flow for 30 min for pre-diffusion of compound and then incubated aerobically at 35 °C and examined after 24 h [25, 26]. The diameter of the zone of inhibition produced by each agent were measured with a ruler and compared with those produced by the commercial antibiotic Streptomycin.

2.5.2 Fungal susceptibility screening

The antifungal activity of the synthesized compounds was tested using agar well diffusion method. The potato dextrose agar plates were inoculated with each fungal culture (10 days old) by point inoculation. A well of about 6.0 mm diameter with sterile cork borer was aseptically punched on each agar plate. The synthesized test compound (100 µg/100 µL) was introduced into the well; a negative control well was too made with 100 µL of the solvent DMSO and 100 µg/100 µL Nystatin as the positive control. The plates were kept in laminar flow for 30 min for pre-diffusion of compound to occur and then incubated at 28 °C for 48 h. Resulting zone of inhibition (in mm) was measured using a Hi media zone scale [27].

2.6. CT-DNA interaction studies

All experimental involving CT DNA were performed in HCl/NaCl (5:50 mM) buffer solution (pH = 7.24). Tris-HCl was prepared using deionized and sonicated triple distilled water and kept at 4 °C for 3 days. The absorption ratio of CT DNA solutions A_{260}/A_{280} was 1.9:1, indicating that the DNA was sufficiently free from protein [28]. The CT DNA concentration was determined via

absorption spectroscopy using the molar absorption coefficient of $6600 \text{ M}^{-1} \text{ cm}^{-1}$ (260 nm) for CT DNA [29].

Stock solutions of metal complexes were prepared by dissolving them in dimethyl sulphoxide (DMSO) and suitably diluting them with the corresponding buffer to the required concentrations for all experiments. The extent of DMSO in the final concentration didn't exceed 0.1 % in the tested solutions. At this concentration, DMSO was not found to have any effect on CT DNA conformation.

Absorption titration experiments were carried out by varying the CT DNA concentration in the range of (0-10 μM) and maintaining the H_2L and its Co(II) Cu(II) and Zn(II) complexes concentration constant at (100 μM). Upon measuring the absorption spectra, equal amount of DNA was added to both the complex solution and the reference solution to eliminate the absorbance of DNA itself. The reference solution was the corresponding buffer solution. Absorbance values were recorded after each successive addition of CT DNA solution and equilibration for ~ 10 min. Each sample was measured three times and an average value was calculated. The absorption data were analyzed for an evaluation of the intrinsic binding constant K_b of the complexes with CT DNA.

DNA competitive binding studies with ethidium bromide solution (EB) were carried out keeping the concentration of EB (30 μM) and CT DNA (200 μM) constant and varying the concentration of the complexes (0-100 μM). Before measurements, the resulting solutions were shaken up and incubated for 30 min. The emission spectra were recorded in the wavelength range of 500-700 nm at 595 nm (478 nm excitation wavelength).

2.7. Computational methods:

All computations were carried out using Gaussian 09W software package [30]. Molecular geometries of all the studied complexes were fully optimized using B3LYP/LANL2DZ [31-33]. No symmetry constrains were applied during the geometry optimization [34, 35] [. The choice of this basis set was due to its flexibility and the fact that the diffused p functions on the H-atom tend to compensate the anharmonic effects of the CH and NH stretches. By using HOMO and LUMO energy values for complexes, electronegativity and chemical hardness can be calculated as follows: $\chi=(I+A)/2$ (electronegativity), $\eta=(I-A)/2$ (chemical hardness), $S=1/2\eta$ (chemical softness) where I and A are ionization potential and electron affinity, and $I= -E_{\text{HOMO}}$ and $A= -E_{\text{LUMO}}$, respectively [36, 37]. NBO calculations have been performed at the B3LYP/ LANL2DZ

level using NBO 3.1 program as implemented in the Gaussian 09W software package in order to qualitatively measure the intramolecular delocalization in the studied system. Throughout this work MOs were constructed using the Gauss-view 5.08 visualization program [38]. The total static dipole moment (μ), the mean polarizability $\langle\alpha\rangle$, the anisotropy of the polarizability $\Delta\alpha$ and the mean first hyperpolarizability $\langle\beta\rangle$ using the x, y, z components were calculated by using the following equations [39-41]:

$$\mu = (\mu_x^2 + \mu_y^2 + \mu_z^2)^{\frac{1}{2}} \quad (1)$$

$$\alpha = \frac{\alpha_{xx} + \alpha_{yy} + \alpha_{zz}}{3} \quad (2)$$

$$\Delta\alpha = \sqrt{\frac{(\alpha_{xx} - \alpha_{yy})^2 + (\alpha_{yy} - \alpha_{zz})^2 + (\alpha_{zz} - \alpha_{xx})^2}{2}} \quad (3)$$

$$\langle\beta\rangle = \beta_x^2 + \beta_y^2 + \beta_z^2 \quad (4)$$

where

$$\beta_x = \beta_{xxx} + \beta_{xyy} + \beta_{xzz} \quad (5)$$

$$\beta_y = \beta_{yyy} + \beta_{xxy} + \beta_{yzz} \quad (6)$$

$$\beta_z = \beta_{zzz} + \beta_{xxz} + \beta_{yyz} \quad (7)$$

3. Results and Discussion

3.1. Schiff base characterization

The elemental analyses (C, H, N, S) data with molecular formula of the Schiff base ligand, H₂L, are presented in Table 1. The results are in good agreement with the suggested molecular formula, C₁₇H₁₃NOS. The structure of the Schiff base H₂L is represented in Scheme 1. The mass spectrum of the ligand (Fig. 1) shows a well-defined parent peak at $m/z = 280$ (P⁺), with a relative intensity of 17%. The IR spectrum (KBr pellets) of the solid H₂L free ligand (Fig. 2) displayed a strong, sharp band at 3262 cm⁻¹ corresponded to the stretching frequency of NH⁺ group [18, 42] where a proton transferred from SH group to the nitrogen of azomethine as

suggested in literature [22]. This fact is identical with the present work where no stretching frequency band due to SH group is displayed. In addition, the IR spectrum of the solid ligand showed no band due to the OH stretching frequency referred to the presence of intramolecular hydrogen bonding between the OH and S-moieties [43] (**Scheme 2**). Furthermore, the IR spectrum displayed stretching bands at 1622, 1267 and 708 cm^{-1} due to C=N, C-O and C-S moieties, respectively [44]. The ^1H NMR spectrum of a solution of the Schiff base ligand in DMSO displayed singlets at 10.54 and 8.44 ppm due to OH and CH=N protons, respectively (Fig 3-a, Table 3). The OH singlet was disappeared in ^1H NMR spectrum in the presence of D_2O (Fig 3-b). The singlet of SH signal was expected to be confused through the aromatic multiplets. So, the ^1H NMR spectrum was expanded in the aromatic region. Accordingly, in the absence of D_2O (Fig 4-a) a broad singlet signal at 7.00 ppm was appeared due to SH proton. This signal disappeared in presence of D_2O (Fig. 4-b). These results confirmed the presence of SH and OH protons at 7.00 ppm and 10.54 ppm in the ^1H NMR spectrum of the ligand solution.

3.2. Complexes characterization

Reaction of the metal ions Co(II), Cu(II), Zn(II), Cd(II) and Hg(II) with N-(2-hydroxynaphthylidene)-2-aminothiophenol (H_2L) in ethanol resulted in the formation of the five complexes $[\text{Co}(\text{HL})_2]\text{H}_2\text{O}$, $[\text{Cu}(\text{HL})_2]$, $[\text{Zn}(\text{HL})_2]$, $[\text{Cd}(\text{HL})_2]$ and $[\text{Hg}(\text{HL})\text{Cl}]$ (**1-5**). The conductivity measurements of the ligand and its complexes in DMF proved non-electrolyte character (Table 1). The IR spectra of the metal complexes showed suitable shifts in the characteristic bands of the ligand as result of complex formation (Table 2). The IR spectra of the studied complexes exhibited $\nu(\text{OH})$ stretching frequency band in the range 3410-3463 cm^{-1} indicating the presence of the OH group in the complex. The broad stretching band at 3463 cm^{-1} in the cobalt complex was referred to the presence of H_2O moiety. The $\nu(\text{OH})$ band of the OH group in cobalt complex may be confused within the broad band of the H_2O molecule. The ^1H NMR spectra of the three diamagnetic complexes **3**, **4** and **5** displayed OH singlets at 9.45, 9.27 and 9.50 ppm, respectively. The higher field shift of these singlets with respect to that of the ligand (10.54 ppm) indicates the coordination of the metal ions to H_2L ligand via the oxygen of the OH group without deprotonation. Furthermore, the IR spectrum of the complexes exhibited $\nu(\text{C}=\text{N})$, $\nu(\text{C}-\text{O})$ and $\nu(\text{C}-\text{S})$ bands in the ranges 1602-1616 cm^{-1} , 1209-1216 cm^{-1} and 679-720 cm^{-1} , respectively, with lower shifts referred to the corresponding values for the ligand. These results indicate the coordination of azomethine nitrogen, hydroxyl oxygen and sulfur of thiol

group of the H₂L Schiff base to the metal ions in the complexes [14]. This is confirmed by the appearance of stretching frequency bands, in the IR spectra of the metal ion complexes, corresponding to M-O, M-N and M-S bonds in the ranges 487-505 cm⁻¹, 450-469 cm⁻¹ and 407-427 cm⁻¹, respectively, (Table 2).

The cobalt and copper complexes showed paramagnetic properties and gave no ¹H NMR spectrum. Magnetic susceptibility measurements of these two complexes at 298 K showed values of 8.56×10⁻⁶ e.m.u.g⁻¹ for cobalt complex and 1.31×10⁻⁶ e.m.u.g⁻¹ for copper complex with an effective magnetic moment (μ_{eff}) of 3.61 BM and 1.40 BM, respectively. The μ_{eff} value of the cobalt complex indicated a high spin *d*⁷ electronic configuration. This electronic configuration is in accordance with +2 formal oxidation state of the cobalt in the complex. Moreover, the μ_{eff} value of the copper complex indicated a high spin *d*⁹ electronic configuration. This electronic configuration is in accordance with +2 formal oxidation state of copper in the complex. Accordingly, the studied metal complexes may have the structures represented in **Scheme 3**.

3.3. Thermogravimetric analysis

The thermal studies of the cobalt, copper, zinc, cadmium, and mercury complexes were carried out using thermogravimetry (TG) and differential thermogravimetry (DTG) techniques. The TG data of the reported complexes were listed in Table 4 and plotted as shown in Figures (S1-S5). The TG plot of CoC₃₄H₂₄N₂O₂S₂(H₂O) displayed three resolved and well-defined decomposition steps in the temperature range 92-879 °C. The first decomposition step occurred in the temperature range 92-190 °C, with a net weight loss of 2.63%, could be due to the elimination of one H₂O molecule which confirms the presence of a hydrated water molecule in the complex. The second decomposition step occurred in the temperature range 206-548 °C with a net weight loss of 59.56 % was due to the loss of a C₂₄H₁₂N₂SO moiety. On the other hand, the third decomposition step (548-879 °C, 28.38 %) was due to the elimination of C₁₀H₁₂SO species to leave metallic residue of cobalt.

The TG plot of the CuC₃₄H₂₄N₂O₂S₂ complex displayed also three decomposition steps in the temperature range 200-968 °C. The first decomposition step occurred in the temperature range 200-387 °C with a net weight loss of 30.87 % corresponded to the elimination of a C₁₅H₁₂ moiety. On the other hand, the second decomposition peak occurred in the temperature range 389-512 °C with a weight loss of 19.63 % and corresponded to the material decomposition of

C₂H₈N₂. In addition, a third decomposition step (514-968 °C, 39.83 %) was due to the elimination of C₁₄H₄S₂O species to give finally CuO + 3C solid residue.

The ZnC₃₄H₂₄N₂O₂S₂ complex was found to thermally decomposed in three well-defined steps in the temperature range 150-999 °C. In the first decomposition step occurred in the temperature range 150-387 °C with a net weight loss of 15.68% and corresponded to the elimination of two C₆H₉N species. The second decomposition step (388-528 °C, 30.69 %) was due to the elimination of two C₉H₆NS₂ species. The third decomposition peak occurred in the temperature range 528-999 °C (weight loss 24.47 %) could be due to the elimination of a C₁₁H₉O moiety to leave ZnO + 8C as a residue.

The CdC₃₄H₂₄N₂O₂S₂ complex decomposed in three well-defined steps with a total mass loss of 100 %. The first decomposition peak occurred in the temperature range 150-378 °C with mass loss of 58.05% corresponded to the loss of C₂₉H₁₁N₂ moiety. The second decomposition step (379-578 °C, 25.33 %) was due to the elimination of C₅H₁₃O₂S₂ species. On the other hand, the third decomposition step occurred in the temperature range 578-999 °C with a weight loss of 16.62 % corresponded to the elimination of metallic cadmium leaving no solid residue.

The TG plot of the HgC₁₇H₁₂NOSCl complex displayed two decomposition steps in the temperature range 150-858 °C. The first decomposition step occurred in the temperature range 150-261 °C with a net weight loss of 35.89 % corresponded to the elimination of a C₁₃H₁₀O moiety. A second decomposition peak occurred in the temperature range 261-858 °C with a weight loss of 63.88 % corresponded to the material decomposition of [C₄H₂NSCl + Hg] giving no solid residue.

3.4. Kinetic data

The Coats-Redfern relation [45] (equation 1) was employed in this work to evaluate the kinetic and thermodynamic activation parameters (E^* , H^* , S^* and G^*) of the decomposition processes of the reported complexes.

$$\log \left[\frac{\log \frac{W_{\infty}}{W_{\infty} - W}}{T^2} \right] = \log \left[\frac{AR}{\phi E^*} \left(1 - \frac{2RT}{E^*} \right) \right] - \frac{E^*}{2.303RT} \quad (8)$$

W_{∞} is the total mass loss of the decomposition reaction, W is the mass loss up to temperature T , ϕ is the heating rate while R is the gas constant. The plot of the left-hand side of equation (8) against $1/T$, considering $1-2RT/E^* \cong 1$, would give a straight line with definite slope and intercept. The activation energy (E^*) and the pre-exponential factor, A , could be calculated from the slope and the intercept of this line, respectively. On the other hand, the entropy (S^*), enthalpy (H^*) and free energy change (G^*) of activation, were calculated using the following equations:

$$S^* = 2.303 \left(\log \frac{Ah}{kT} \right) R \quad (9)$$

$$H^* = E^* - RT \quad (10)$$

$$G^* = H^* - TS^* \quad (11)$$

where, (h) is Planck's constant and (k) is Boltzman constant. The kinetic parameters are listed in Table 5. The activation energies of decomposition were in the range 4.60-218.34 kJ mol⁻¹. The high positive values of the G^* reflect the high stability of the investigated complexes. This behavior corresponded to the covalent character of the complexes [46, 47]. On the other hand, the negative values of S^* for the degradation process (-5.40 to -283.26 kJ mol⁻¹) reveal more ordered activated complex and lower rate for the decomposition reactions than normal ones [48, 49].

3.5. Antimicrobial activity

The ligand (H_2L) and its metal complexes were screened against the bacterial strains *B. subtilis*, *S. aureus*, *E. coli*, *K. pneumoniae* and fungal strains *C. albicans*, *A. niger*. The results of inhibition are compared with standard antibacterial drug Streptomycin and antifungal drug Nystatin. The antimicrobial activity of H_2L ligand and its complexes bacteria and fungi is summarized in Table 6. The antibacterial activities of Cd(II) and Hg(II) complexes weren't studied for their toxicity. It was clear that, Co(II), Cu(II) and Zn(II), complexes exhibit significant activity against all bacterial and fungal strains, this may be due to the presence of the imine group may be one of the reasons for the biocidal action of both the ligand and metal complexes. Among the reported complexes, Cu(II) complex shows the highest biocidal activity than other complexes. Generally, all complexes show higher antimicrobial properties compared to the free H_2L ligand. This behavior was explained by Overtone's concept and Tweedy's

chelation theory [50-52]. Upon chelation operates, the polarity of the metal ion decrease extensively and the delocalization of π -electrons increase on the whole chelation ring for the en towards enhancement lipophilicity of complexes. This could results in better penetration of the complexes into lipid membranes. This can further block the metal binding sites on the enzymes of the microorganisms. Thus, in general, the complexes show better activity than their Schiff base ligand.

3.6. DNA binding studies

3.6.1. Absorption spectral studies

The application of UV-Vis absorption spectroscopy technique is one of the most meted to study the binding mode of DNA with small molecules [53]. The electronic absorption spectra of the investigated ligand and its complexes consist of two or three well-resolved bands in the range of 259-500 nm. The high-energy absorption band appeared in the spectra of the ligand and its complexes below 350 nm are assigned to π - π^* and n - π^* transitions [54] and the band observed above 400 nm in the complexes spectra may be assigned to LMCT transition, usually observed in metal Schiff base complexes containing phenolated ligands due to “phenolate-to-M” charge transfer [55] or d-d transition. The absorption spectra of H₂L and its Co(II) and Cu(II) complexes in the absence and presence of CT DNA are given in Fig 6. With increasing concentration of CT DNA, all the complexes showed hypochromicity and a red-shifted charge transfer peak maxima, indicating the complexes are actively in associating with CT DNA. These spectral characteristics obviously suggested that the titled complexes most likely interact with DNA through a mode of stacking interaction between the aromatic chromophore of the complexes and the base pairs of DNA. For the quantitative investigation of the binding strength of the ligand and its complexes to CT DNA, the intrinsic binding constants K_b of the complexes with CTDNA were calculated using the following function equation [56]:

$$\frac{[\text{CT DNA}]}{(\epsilon_a - \epsilon_f)} = \frac{[\text{CT DNA}]}{(\epsilon_b - \epsilon_f)} + \frac{1}{K_b(\epsilon_a - \epsilon_f)} \quad (12)$$

where [CT DNA] is the concentration of CT DNA in base pairs, ϵ_a is the extinction coefficient obtained by calculating $A_{\text{obs}}/[\text{compound}]$, ϵ_f corresponds to the extinction coefficient of the compound in its free form and ϵ_b refers to the extinction coefficient of the in the fully bound form, respectively. In plots $[\text{CT DNA}]/(\epsilon_a - \epsilon_f)$ versus [CT DNA] (Fig.5, inset), the intrinsic binding constants (K_b) value, given by the ratio of the slope to the intercept of the linear fit of the

data, were found to be $0.722 \times 10^4 \text{ M}^{-1}$, $2.685 \times 10^4 \text{ M}^{-1}$, $3.078 \times 10^4 \text{ M}^{-1}$, $1.999 \times 10^4 \text{ M}^{-1}$, for H₂L and its Co(II), Cu(II) and Zn (II) complexes, respectively, indicating a moderate intercalation between the complexes and CT DNA. These (K_b) values are much smaller than the typical classical intercalators (e.g. EB-DNA, $\sim 10^6 \text{ M}^{-1}$) [57] and have the same level as those of some well-established intercalation agents ($\sim 10^4$) [58, 59]. The K_b value (Table 7) revealed that the comparative binding strength of the complexes with CT-DNA were in the order Cu(II) complex > Co(II) complex > H₂L, suggesting that Cu(II) intercalates more strongly than other complexes.

3.6.2. Fluorescence spectral studies

Ethidium bromide (EB) was used to investigate the potential DNA binding mode of the ligand and its Co(II), Cu(II) and Zn (II) complexes. EB emits intense fluorescence at 595 nm in the presence of CT DNA due to high intercalation between the adjacent DNA base pairs. The addition of a second small molecule which binds to DNA better than EB would suppress the DNA-induced EB emission [60]. The extent of quenching of the fluorescence of EB bound to DNA would reflect the extent of the DNA binding of the second molecule. The ligand, the complexes, and CT DNA independently or in combination do not give luminescence spectra in the buffer and DMSO. The emission spectra of DNA-bound EB in the absence and the presence of the ligand and its Co(II) Cu(II) and Zn(II) complexes are shown in Fig. 6. It was clearly seen that, the addition of the reported compounds to CT-DNA pretreated with EB caused an appreciable reduction in emission intensity, indicating that the complexes bind to DNA at the sites occupied by EB. The quenching of the EB bound to DNA by the complex is in agreement with the linear Stern–Volmer Eq. [61]:

$$\frac{I_0}{I} = 1 + K_{sv} \frac{[\text{Compound}]}{[\text{CT DNA}]} \quad (13)$$

where I_0 and I represent the fluorescent intensities in the absence and presence of the complex, respectively, and K_{sv} is the linear Stern-Volmer quenching constant. The K_{sv} value is obtained from the slope of the I_0/I versus $[\text{Compound}]/[\text{CT DNA}]$ linear plot (Fig. 6, inset) and is found to be 0.67, 1.45, 1.98 and 1.03 for H₂L, Co(II), Cu(II) and Zn(II) complexes, respectively, indicating that, the CT DNA binding affinity of Cu(II) complex is higher than those of other complexes. Also, the data revealed that DNA-bound EB can be more readily replaced by the complexes in the order Cu(II) complex > Co(II) complex > Zn(II) complex > H₂L, which is consistent with the above UV-Vis observations.

3.7.

Molecule orbital calculations

The optimized geometrical parameters (bond lengths, bond angles and dihedral angles), natural charges on active centers and energetic of the ground state for the studied complexes were computed and analysed. From the elemental analysis and spectroscopic data, metal ions coordinated to the ligand via N, O and S-atoms forming the complexes. Two ligand moieties used in the coordination with Co(II), Cu(II), Zn(II), Cd(II) forming $[M(HL)_2]$ complexes, whereas, Hg(II) coordinated with one moiety of the ligand to form $[Hg(HL)Cl]$ complex.

3.7.1 Geometry of the complexes

Tables 8, 9 and Fig. 7 present the optimized geometry, numbering system, vector of the dipole moment, energetic, dipole moment, bond lengths, bond angles and dihedral angles of all metal complexes studied in this work. In Co(II), Cu(II), Zn(II) and Cd(II) complexes, the metal ion coordinates with O40,C28,C27,C31,N32 and N52,C11,C10,C5,O19 to form a six-member ring and with S39,C32,C33,N32 and N52,C53,C54,S59 to form a five member ring. In case of Hg-complex, the ion coordinated with S27,C22,C21,N20 to form five member ring and with O19,C5,C10,C11,N20 to form six member ring. Therefore, distortion from regular octahedral geometry is expected for all the studied complexes. Most M-N, M-S and M-O bonds show elongation upon complexation. The length of the coordinate covalent bonds between metal and ligand site, i.e. M-N, M-S and M-O, are too long compared to the typical MX bond lengths [62]. The too long M-O, M-S and M-N bonds in the studied complexes mean that the ionic character of these bonds is small. The calculated values of bond angles between metal ion and binding sites (Tables 8 and 9) N32MS39, N32MO40, O40MS59, S59MN52, N52MO19 and O19MS39 vary between 45° and 129° which compare nicely with the experimental data as obtained from X-ray analysis for Oh complexes [63], which indicate a distorted octahedral geometry. The dihedral angles around metal ion, i.e. MN32C31C27, MO40C28C27, MO40C28C29 and MN32C31H47, are far from 0° or 180° which indicate that the metal ion is not in the same molecular plane of the ligand.

3.7.2 Natural charges and natural population

The natural population analysis performed on the electronic structures of the studied complexes clearly describes the distribution of electrons in various sub-shells of their atomic orbits. The natural charges on the coordinating sites in the core, valence and rydberg sub-shells and natural electronic configuration of the metal in the studied complexes are presented in Tables 10 and 11 .

The most electronegative centers are accumulated on N12, S19, O63, N43, S50 and O51. These electronegative atoms have a tendency to donate electrons. Whereas, the most electropositive atoms are Co, Cu, Zn, Cd and Hg have a tendency to accept electrons. The central metal ion in the Co-complex received 1.6681e from the donating sites of the ligands with electronic configuration $3d^{7.75}$. In case of Cu-, Zn-, Cd-, and Hg-complexes the central metal ions received 1.1492e ($3d^{9.37}$), 0.7358e ($3d^{9.98}$), 0.76194e ($4d^{9.99}$) and 0.9307e ($5d^{9.97}$) from the active sites of the ligands respectively. Total Lewis (effective core, core and valence Lewis) and total non-Lewis (valence non-Lewis and rydberg non-Lewis) of the studied complexes are presented in Table 12.

3.7.3 Global reactivity descriptors

They include HOMO, LUMO, energy gap (Eg), chemical hardness (η), electronegativity (χ), chemical potential (V), electron affinity (A), ionization potential (I) and chemical softness(S). The frontier molecular orbital (FMO) energies of the studied complexes were calculated using B3LYP/LANL2DZ and presented in Fig. 8. HOMO energy characterizes the electron donating ability, while LUMO energy characterizes the electron withdrawing ability. Energy gap (Eg) between HOMO and LUMO characterizes the molecular chemical stability which is a critical parameter in determining molecular electrical transport properties because it is a measure of electron conductivity. The results in Fig. 8 and Tables 9 and 13 indicate that the smaller the energy gap the easier the charge transfer and the polarization occurs within the molecule. Furthermore, the order of increasing reactivity is: Co \gg Zn > Cu > Cd > Hg. Using HOMO and LUMO energies, ionization potential and electron affinity can be expressed as $I \sim -E_{\text{HOMO}}$, $A \sim -E_{\text{LUMO}}$ as shown in Tables 9 and 13. The variation of electronegativity (χ) values is supported by electrostatic potential, for any two molecules, where electron will be partially transferred from one of low χ to that of high χ . The results show that the order of decreasing χ (increasing CT within the molecules) is: Cu > Hg > Zn > Cd > Co.

The chemical hardness (η) = (I-A)/2, electronegativity (χ) = (I+A)/2, chemical potential (V) = - (I+E)/2 and chemical softness(S) = 1/2 η values are calculated and presented in Tables 9 and 13. The results of small η values for the studied compounds reflect the ability of charge transfer inside the molecule. Therefore, the order of increasing the charge transfer within the molecule is: Co > Hg > Zn > Cd > Cu. Considering η values, the higher the η values, the harder is the molecule and vice versa.

3.7.4-Non-linear optical properties (NLO)

No experimental or theoretical investigations were found addressing NLO for the studied complexes; therefore, this triggered our interest to undertake this study. NLO properties is the key functions of frequency shifting, optical modulation, switching, laser, fiber, optical materials logic and optical memory for the emerging technologies in areas such as telecommunications, signal processing and optical inter connections [64-66]. In order to investigate the relationship between molecular structure and NLO, the polarizabilities and hyperpolarizabilities of the studied complexes are calculated using B3LYP/LANL2DZ. Total static dipole moment (μ), the mean polarizability α , the anisotropy of the polarizability $\Delta\alpha$ and the mean first-order hyperpolarizability (β) of the studied complexes are listed in Table 14. The polarizabilities and first-order hyperpolarizabilities are reported in atomic units (a.u.), the calculated values have been converted into electrostatic units (esu) using conversion factor of 0.1482×10^{-24} esu for α and 8.6393×10^{-33} esu for β . Urea is a standard prototype used in NLO studies. In this study, Urea is chosen as a reference as there were no experimental values of NLO properties of the studied complexes. The magnitude of the molecular hyperpolarizability β is one of the key factors in NLO system. The analysis of the β parameter show that Hg-complex is ~ 12 times higher than (UREA), while Co(II), Cu(II), Zn(II), Cd(II) complexes are 7, 2, 8 and 5 higher than the reference respectively. Therefore, the studied complexes are an efficacious candidate for NLO materials.

4. Conclusions

In this work, the reaction of some transition metal ions Co(II), Cu(II), Zn(II), Cd(II) and Hg(II) with a Schiff base ligand has been studied. Elemental analyses, IR, ^1H NMR, magnetic measurement, molar conductance, and thermal analysis suggested the five complexes; $[\text{Co}(\text{HL})_2]\text{H}_2\text{O}$, $[\text{M}(\text{HL})_2]$ (M= Cu, Zn and Cd) and $[\text{Hg}(\text{HL})\text{Cl}]$. Kinetic and thermodynamic parameters reflect the high stability of the complexes. The parent ligand (H_2L) and its metal complexes were screened against some bacteria and fungi strains. Furthermore, DNA binding interaction with calf-Thymus DNA (CT DNA) have been elucidated by electronic absorption spectral titration and steady state fluorescence competition studies and the data revealed that, the complexes bind to CT-DNA in the order Cu(II) complex > Co(II) complex > Zn(II) complex > H_2L . The molecular geometry of the studied complexes in the ground state has been calculated by using DFT-B3LYP/LANL2DZ level of theory. The optimized structure of the studied

complexes are non-linear with the metal ion is not in the same plane as the donating sites. The HOMO-LUMO energy gap helped in analyzing the chemical reactivity, hardness, softness, chemical potential and electro negativity. Natural charge distribution of the studied complexes was studied which indicated the electronic charge distribution in the complexes. The calculated dipole moment and first order hyperpolarizability results indicate that the complexes have a reasonable good non-linear optical behavior.

References

- [1] J. Collman, L.S. Hegedus, Principles and Application of Organotransition Metal Chemistry, University Science Book, California, 1980.
- [2] M.M. Taqui Khan, N.M. Khan, R.I. Kureshy and A.B. Boricha, *J. Coord. Chem.* 43 (1998) 31.
- [3] D. Chen, A.E. Martell, *Inorg. Chem.* 26 (1987) 1026-1030.
- [4] J. Zhao, B. Zhao, J. Liu, W. Xu, Z. Wang, *Spectrochim. Acta A* 57 (2001) 149-154.
- [5] M.Z. Zgierski, A. Grabowska, *J. Chem. Phys.* 113 (2000) 7845-7852.
- [6] W.J. Sawodny, M. Riederer, *Angew. Chem. Int. Edn. Engl.* 16 (1977) 859-860.
- [7] S. Ren, R. Wang, K. Komatsu, P. Bonaz-Krause, Y. Yrianov, C.E. McKenna, C. Csipke, Z.A. Tokes, E.J. Lien, *J. Med. Chem.* 45 (2002) 410-419.
- [8] M.T.H. Tarafder, M.A. Ali, N. Saravanan, W.Y. Weng, S. Kumar, N. Umar-Tsafe, K.A. Crouse, *Trans. Met. Chem.* 25 (2000) 456-460.
- [9] N. Raman, A. Kulandaisamy, K. Jeyasubramanian, *Synth. React. Inorg. Met.-Org. Chem.* 32 (2007) 1582-1610 .
- [10] N. Raman, A. Thangaraja, C. Kulandaisamy, *Trans. Met. Chem.* 28 (2003) 29-36.
- [11] S.A. Ali, A.A. Soliman, M.M. Aboaly, R.M. Ramadan, *J. Coord. Chem.* 55 (2002) 1161-1170.
- [12] R.M. Ramadan, M.S.A. Hamza, S.A. Ali, *J. Coord. Chem.* 43 (1998) 31-39.
- [13] N. Yoshida, H. Oshio, T. Ito, *J. Chem. Soc., Perkin Trans. 2* (2001) 1674-1678.
- [14] S.M. El-Medani, *J. Coord. Chem.* 57 (2004) 115-122.
- [15] R.G. Mohamed, F.M. Elantabli, N.H. Helal, S.M. El-Medani, *Synth. React. Inorg. Met.-Org. Chem.* 45 (2015) 1839-1850.
- [16] A.A. Soliman, W. Linert, *Synth. React. Inorg. Met.-Org. Chem.* 29 (1999) 1133-1151.

- [17] N. Raman, A. Kulandaisamy, K. Jeyasubramanian, *Synth. React. Inorg. Met.-Org. Chem.* 31 (2001) 1249-1270.
- [18] M.M. Aboaly, M.M.H. Khalil, *Spectrosc. Lett.* 34 (2001) 495-504.
- [19] C. Jayabalakrishnan, K. Natarajan, *Trans. Met. Chem.* 27 (2002) 75-79.
- [20] A.A. Soliman, W. Linert, *Thermochim. Acta* 338 (1999) 67-75.
- [21] M.M.H. Khalil, M.M. Aboaly, R.M. Ramadan, *Spectrochim. Acta A* 61 (2005) 157-161.
- [22] A.A. Abdel Aziz, R.G. Mohamed, F.M. Elantabli, S.M. El-Medani, *J. Fluoresc.* 26 (2016) 1927-1938.
- [23] D. Sharma, R.K. Bera, S.K. Sahoo, *Spectrochim. Acta A* 105 (2013) 477-82.
- [24] R. Nair, T. Kalariya, S. Chanda, *J. Biol.* 29 (2005) 41-47.
- [25] C.H. Collins, P.M. Lyne, J.M. Grange, *Microbiol. Methods*, sixth ed., 198, p 410
- [26] M.S. Ali-Shtayeh, R. M Yaghmour, Y.R. Faidi, K. Salem, M.A. Al-Nuri, *J. Ethnopharmacol.* 60 (1998) 265-271.
- [27] R.K. Pundir, P. Jain, *J. Pharm. Res.* 3 (2010) 506-510.
- [28] J. Marmur, *J. Mol. Biol.* 3:2 (1961) 208-218.
- [29] M.E. Reichmann, S.A. Rice, C.A. Thomas, P. Doty, *J. Am. Chem. Soc.* 76 (1954) 3047-3053.
- [30] G.W.T.M. J. Frisch, H.B. Schlegel, G.E. Scuseria, M.A. Robb, J.R. Cheeseman, G. Scalmani, V. Barone, B. Mennucci, G.A. Petersson, H. Nakatsuji, M. Caricato, X. Li, H.P. Hratchian, A.F. Izmaylov, J. Bloino, G. Zheng, J. L. Sonnenberg, M. Hada, M. Ehara, K. Toyota, R. Fukuda, J. Hasegawa, M. Ishida, T. Nakajima, Y. Honda, O. Kitao, H. Nakai, T. Vreven, J. A. Montgomery Jr., J.E. Peralta, F. Ogliaro, M. Bearpark, J.J. Heyd, E. Brothers, K.N. Kudin, V.N. Staroverov, R. Kobayashi, J. Normand, K. Raghavachari, A. Rendell, J.C. Burant, S.S. Iyengar, J. Tomasi, M. Cossi, N. Rega, J.M. Millam, M. Klene, J.E. Knox, J.B. Cross, V. Bakken, C. Adamo, J. Jaramillo, R. Gomperts, R.E. Stratmann, O. Yazyev, A.J. Austin, R. Cammi, C. Pomelli, J.W. Ochterski, R.L. Martin, K. Morokuma, V.G. Zakrzewski, G.A. Voth, P. Salvador, J.J. Dannenberg, S. Dapprich, A.D. Daniels, O. Farkas, J.B. Foresman, J.V. Ortiz, J. Cioslowski, D.J. Fox, Gaussian Inc., Wallingford, CT (2009).
- [31] T. Schaefer, T.A. Wildman, S.R. Salman, *J. Am. Chem. Soc.*, 102 (1980) 107-110.
- [32] T. Schaefer, S.R. Salman, T.A. Wildman, P.D. Clark, *Can. J. Chem.* 60:3 (1982) 342-348.
- [33] A.D. Becke, *J. Chem. Phys.* 98 (1993) 5648-5652.

- [34] S.E. Ulic, C.O.D. Védova, A. Hermann, H.-G. Mack, H. Oberhammer, *J. Phys. Chem. A* 112:27 (2008) 6211-6216.
- [35] A.E. Reed, F. Weinhold, *J. Chem. Phys.*, 78 (1983) 4066-4073.
- [36] R.G. Pearson, *P. Natl. Acad. Sci. USA* 83:22 (1986) 8440-8441.
- [37] A.K. Chandra, T. Uchimara, *J. Phys. Chem. A* 105:14 (2001) 3578-3582.
- [38] X-J. Chen, F. Wu, M. Yan, H.-B. Tian, S.X. Li, X. Shan, K. Wang, Z. Li, K. Xu, *Chem. Phys. Lett.* 472 (2009) 19-22.
- [39] D. Avci, *Spectrochim. Acta A.* 82 (2011) 37- 43.
- [40] D. Avci, A. Başoğlu, Y. Atalay, *Struct. Chem.* 21 (2010) 213-219.
- [41] D. Avci, H. Cömert, Y. Atalay, *J. Mol. Model.* 14 (2008) 161-169.
- [42] M T. Dziembowska, E. Jagodzińska, Z. Rozwadowski, M. Kotfica, *J. Mol. Struct.* 598 (2001) 229-234.
- [43] J. Sandstrom, *Dynamic NMR Spectroscopy*, Academic Press, New York, 1982.
- [44] K. Nakamoto, *Infrared and Raman Spectra of Inorganic and Coordination Compounds*, sixth ed., Wiley, New York, 2009.
- [45] A.W. Coats, J.P. Redfern, *Nature* 201 (1964) 68-69.
- [46] T. Taakeyama, F.X. Quinn, *Thermal Analysis, Fundamentals and Applications to Polymer Science*, John Wiley and Sons, Chichester, 1994.
- [47] O.A.M. Ali, S.M. El-Medani, D.A. Ahmed, D.A. Nassar, *Spectrochim. Acta A* 144 (2015) 99-106.
- [48] A.A. Frost, R.G. Pearson, *Kinetics and Mechanisms*, Wiley, New York, 1961.
- [49] G.G. Mohamed, M.M. Omar, A.M. Hindy, *Turk J. Chem.* 30 (2006) 361-382.
- [50] B.G. Tweedy, *Photopathol.* 55 (1964) 910-914.
- [51] N. Dharmaraj, P. Viswanathamurthi, K. Nataragan, *Trans. Met. Chem.* 26 (2001) 105-109.
- [52] Z.A. Taha, A.M. Ajlouni, W. Al Momani, *J. Lumin.* 132 (2012) 2832–2841.
- [53] J.M. Kelly, A.B. Tossi, D.J. McConnell, C.O. Uigin, *Nucl. Acids Res.* 13 (1985) 6017-6034.
- [54] A.B.P. Lever, *Inorganic Electronic Spectroscopy*, second ed., Elsevier Science, Amsterdam, 1984]

- [55] M.S. Nair, D. Arish, T. Indian I. Metals 64 (2011) 287-292.
- [56] A. Wolfe, G.H. Shimer, T. Meehan, Biochemistry 26 (1987) 6392-6396.
- [57] M. Baldini, M. Belicchi-Ferrari, F. Bisceglie, P.P. Dall' Aglio, G. Pelosi, S. Pinelli, P. Tarasconi, Inorg. Chem. 43 (2004) 7170-7179.
- [58] E.J. Gao, L. Wang, M. Zhu, L. Liu, W.Z. Zhang, Eur. J. Med. Chem. 45 (2010) 311-316.
- [59] M.S. Nair, D. Arish, R.S. Joseyphus, J. Saudi Chem. Soc. 16 (2012) 83-88.
- [60] B.C. Baguley, M. Lebert, Biochemistry 23 (1984) 937-943.
- [61] M.J. Waring, J. Mol. Biol. 13 (1965) 269-282.
- [62] L. Armelao, S. Quici, F. Brigelletti, G. Accorsi, G. Bottaroi, M. Cavazzini, E.Tendello, Coord. Chem. Rev. 254 (2010) 487-505.
- [63] S. S. Zumdahl, Chemistry for Chemical and Biological Sciences, University Science Books, Sausalito, CA, 2000.
- [64] S. Natorajan, G. Shanmugam, S.A. Martin. Cryst. Res. Technol. 43 (2008) 561-564.
- [65] D.S. Chema, J. Zyss, Nonlinear Optical Properties of Organic Molecules and Crystals Academic Press, Orlando, FL, 1987.
- [66] D.S. Bradshaw, D.L. Andrews, J. Nonlinear Opt. Phys. Matter 18 (2009) 285-299.

Figures Captions

Fig. 1. The mass spectrum of the ligand H₂L.

Fig. 2. IR spectrum of the ligand H₂L.

Fig. 3. The ¹H NMR spectrum of the Schiff base ligand H₂L: (a) in absence of D₂O(b)in presence of D₂O.

Fig. 4. The expanded ¹H NMR spectrum of H₂L in the range 6.9-7.1 ppm (a) in absence of D₂O (b)in presence of D₂O.

Fig. 5. Electronic absorption spectra in DMSO solution of H₂L and its Co(II), Cu(II) and Zn(II) complexes (100 μM) in the absence (·····) and presence (—) of increasing amounts of CT-DNA (0-10 μM). Arrows show the changes in absorbance with respect to an increase in the DNA concentration. Inset: linear plot for the calculation of the intrinsic CT DNA binding constant (K_b).

Fig. 6. Emission spectra of CT DNA-bound EB in Tris buffer [EB] = 30 μM, [CT DNA] = 200 μM in the absence (·····) and presence (—) of increasing amounts of H₂L and its Co(II), Cu(II) and Zn(II) complexes (0-100 μM). Arrows show the changes in emission intensity with respect to an increase complex concentration (Inset: plot of Stern-Volmer plot of I₀/I Vs [H₂L]/[CT DNA].and [M(II) complex]/[CT DNA].

Fig. 7. The optimized geometry, numbering system, vector of the dipole moment of the studied complexes using B3LYP/LANL2DZ.

Fig. 8. HOMO-LUMO charge density maps of Co(II), Zn(II) and Hg(II) complexes using B3LYP/LANL2DZ.

Fig. 1.

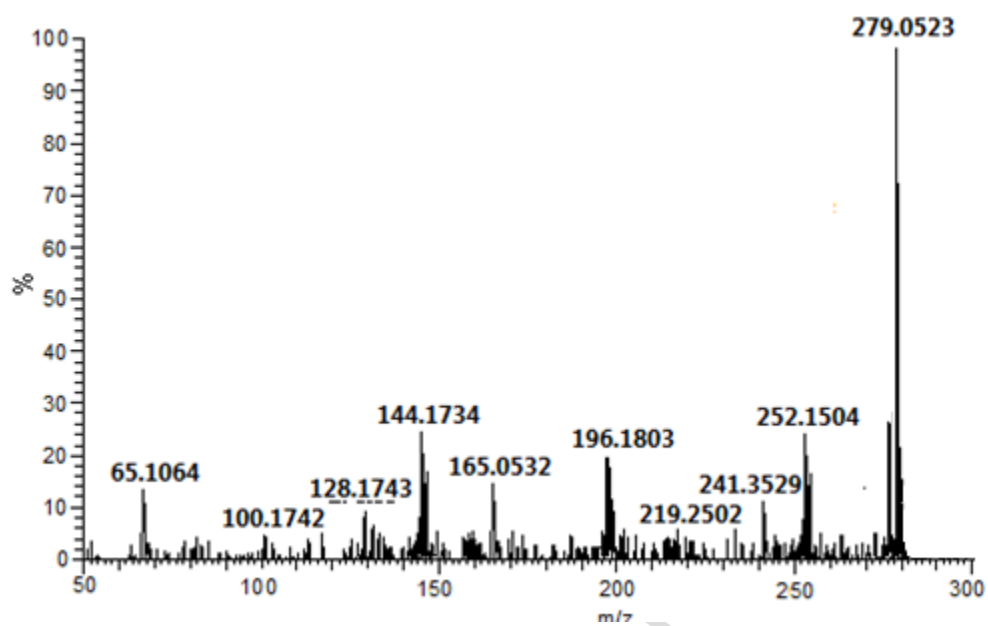
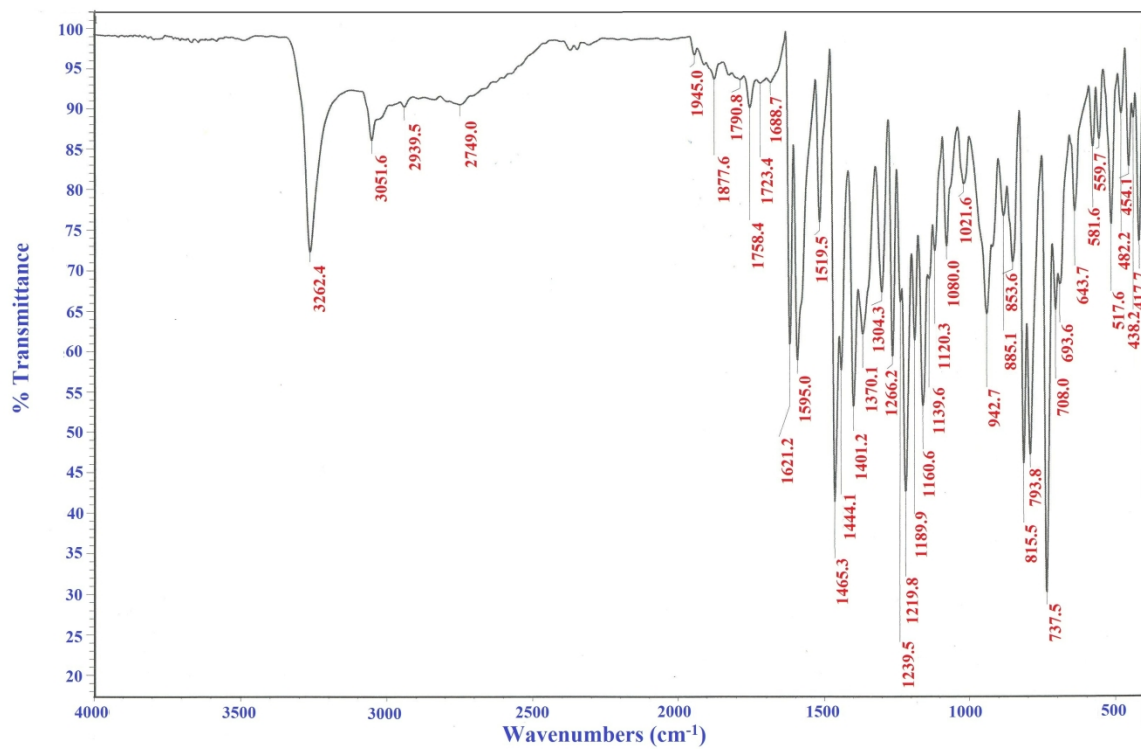


Fig. 2.



ACCEPTED

Fig. 3.

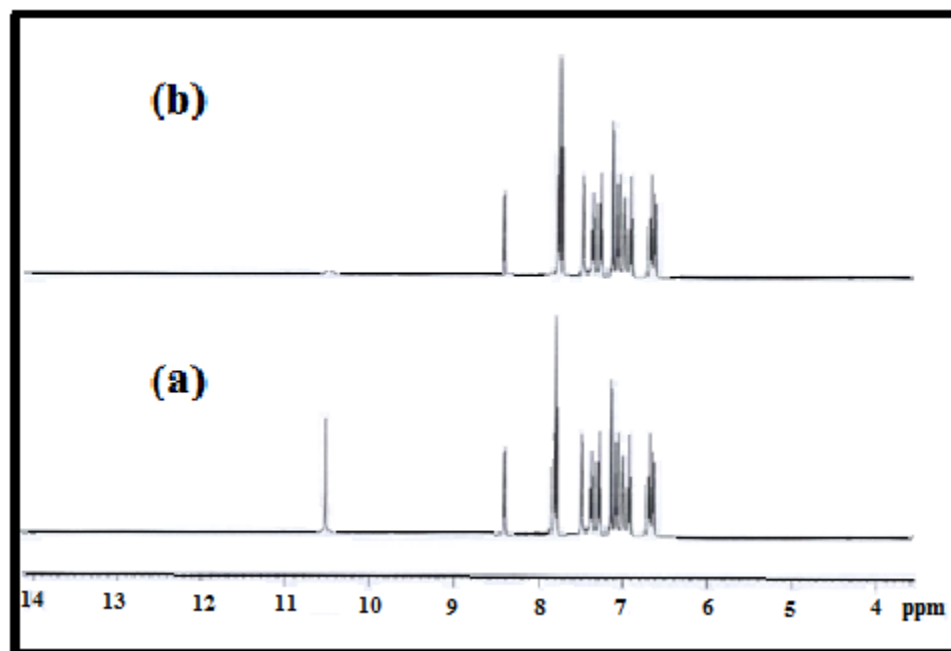


Fig. 4.

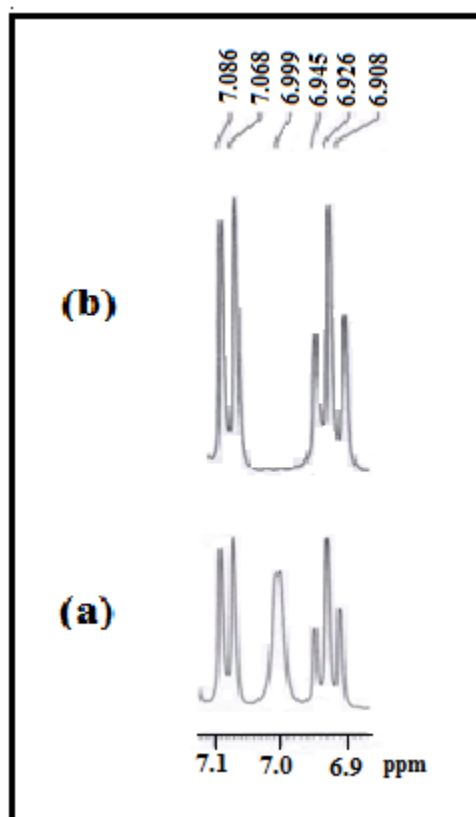


Fig. 5.

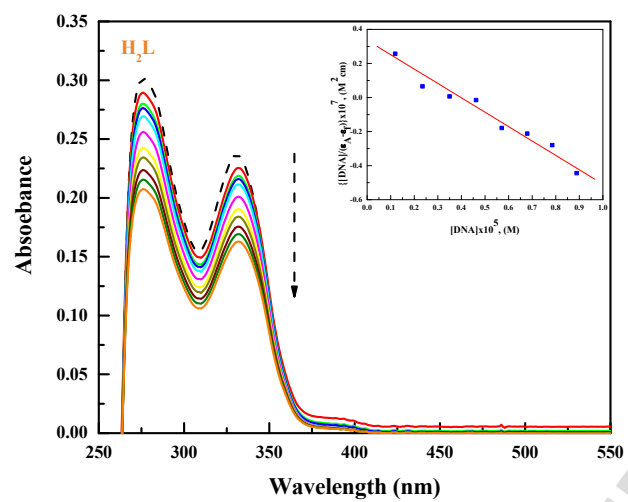
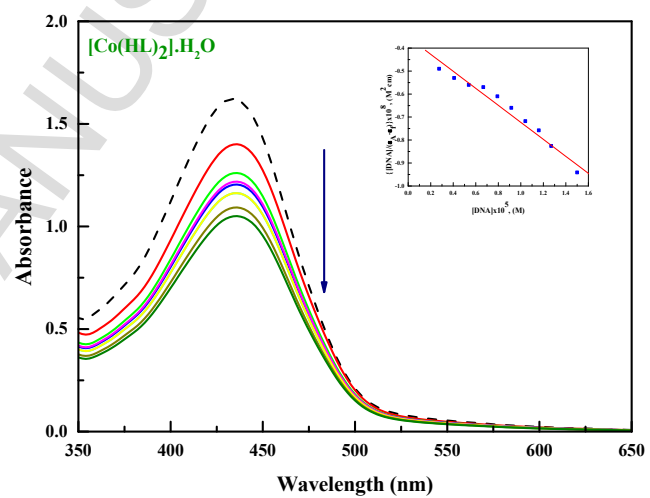


Fig. 6.



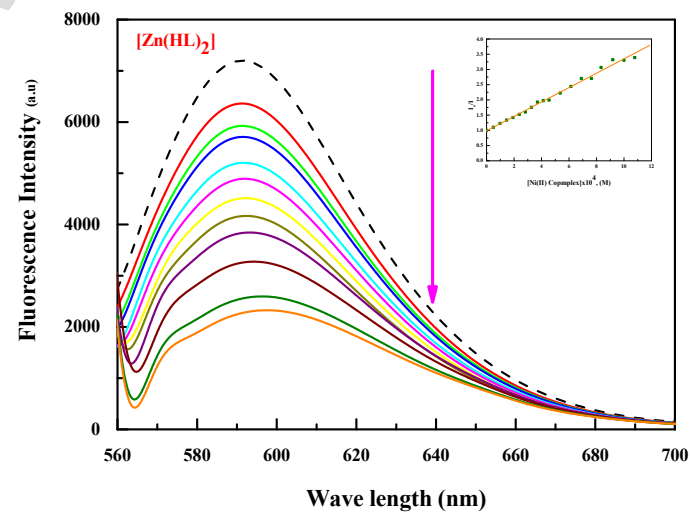
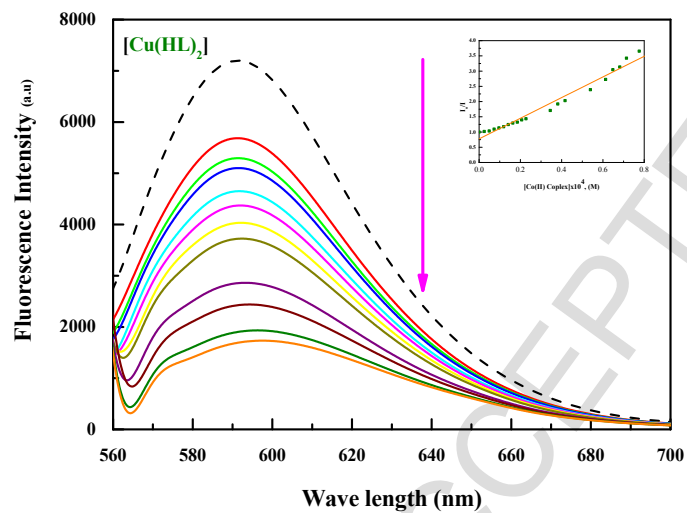
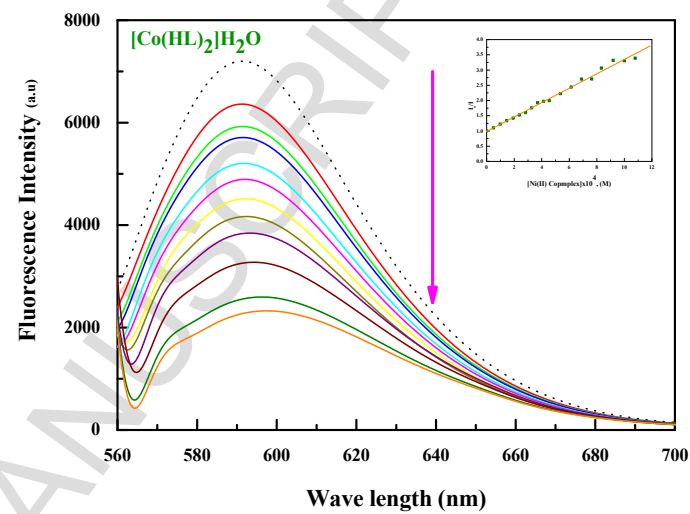
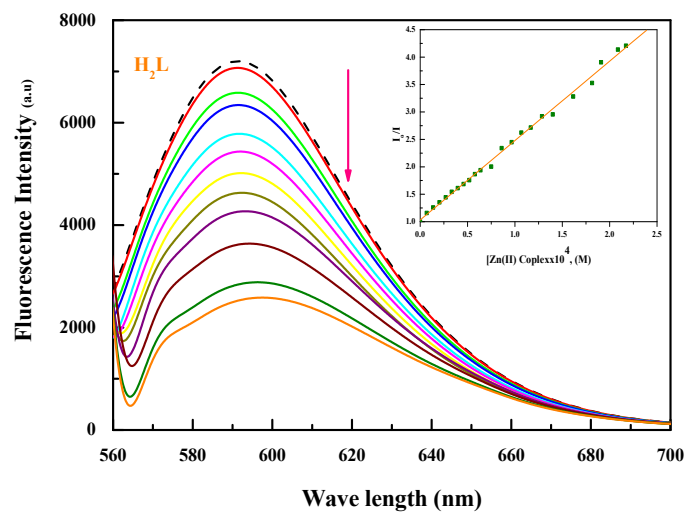


Fig. 7.

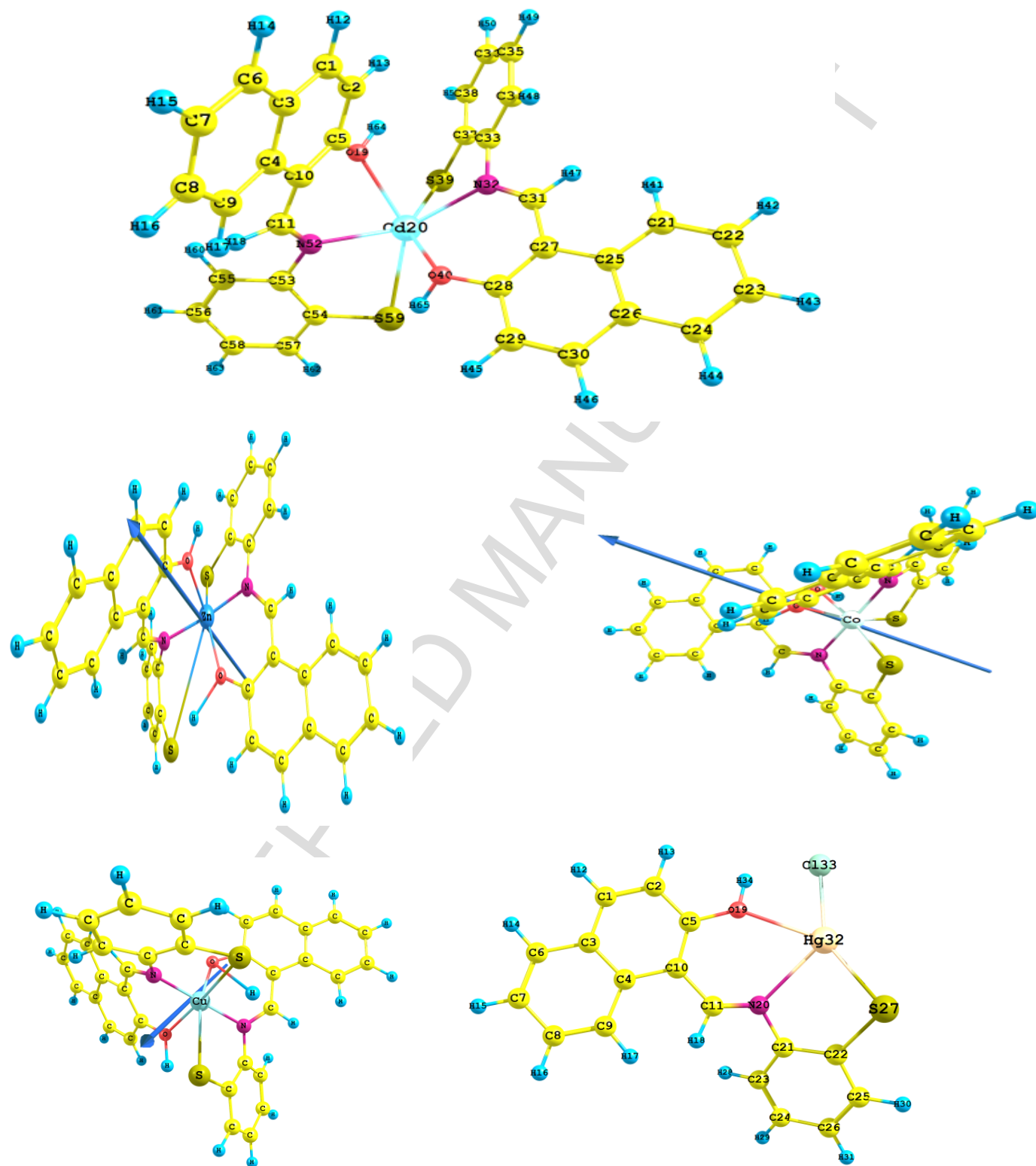
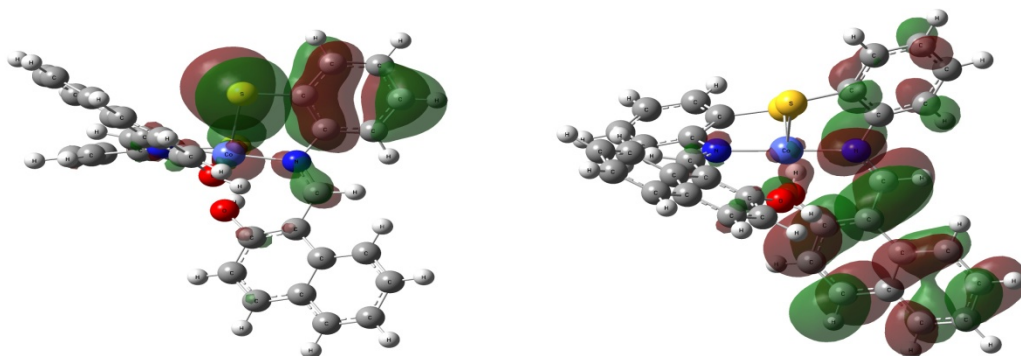
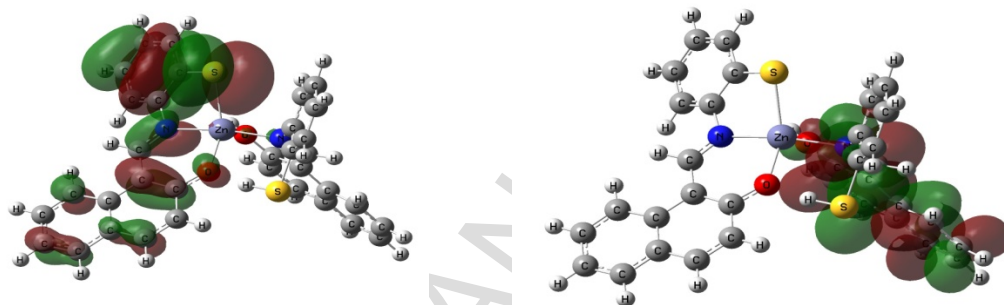


Fig. 8.

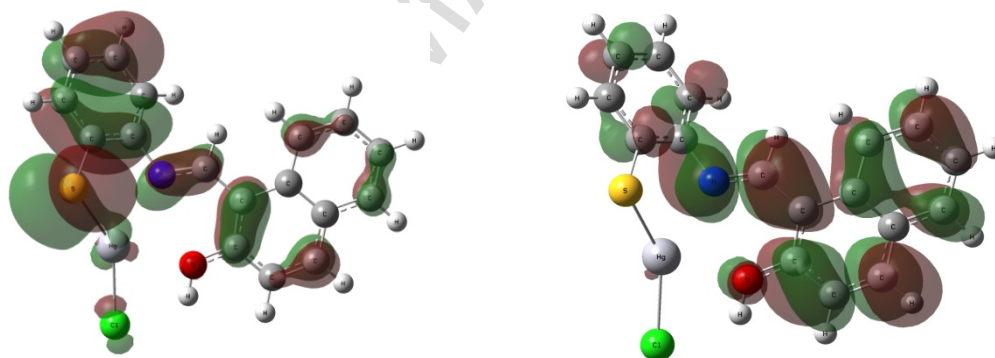
Co(II) Complex



Zn(II) Complex



Hg(II) Complex



HOMO

LUMO

Tables Captions

Table 1 Analytical and physical data of the Schiff base and its complexes.

Table 2 Important IR data for (H₂L) ligand and its complexes.

Table 3 ¹H NMR spectral data of the Schiff bases (II) and their Zn(II), Cd(II) and Hg(II) complexes.

Table 4 Thermal analysis data for Co(II), Cu(II), Zn(II) Cd(II), and Hg(II) complexes (1-5).

Table 5 The kinetic and thermodynamic data of the thermal decomposition of the complexes.

Table 6 Antimicrobial activity of synthesized compounds against microbial strains.

Table 7 UV-Vis absorption properties of H₂L and its Co(II) Cu(II) and Zn(II) complexes (1-3) in presence of CT DNA.

Table 8 Bond lengths, Å, bond angles, degree, and dihedral angles of Co(II) Cu(II), Zn(II) and Cd(II) complexes (1-4) using B3LYP/LANL2DZ.

Table 9 Total energy, energy of HOMO and LUMO, energy gap E_g, global reactivity descriptors, bond lengths, bond angles and dihedral angles for Hg(II) complex (5) using B3LYP/LANL2DZ

Table 10 Natural charge, natural population and natural electronic configuration of metal ions in the studied complexes using B3LYP/LANL2DZ.

Table 11 Natural charge on coordinated atoms of Co(II), Cu(II), Zn(II) and Cd(II) complexes (1-4) using B3LYP/LANL2DZ.

Table 12 Natural population of the total electrons in Co(II), Cu(II), Zn(II) and Cd(II) complexes (1-4) on the sub-shells using B3LYP/LANL2DZ.

Table 13 Global reactivity descriptors of Co(II), Cu(II), Zn(II) and Cd(II) complexes (1-4) using B3LYP/LANL2DZ.

Table 14: Total static dipole moment (μ), The mean polarizability $\langle\alpha\rangle$, The anisotropy of the polarizability $\Delta\alpha$ and The mean first order hyperpolarizability $\langle\beta\rangle$ for Co(II), Cu(II), Zn(II) and Cd(II) complexes (1-4) using B3LYP/LAL2DZ.

Table 1

Compound	C %	H %	N %	S %	M.Wt.	m/z	Color (% yield)	Λ ($\Omega^{-1}\text{mol}^{-1}\text{cm}_2$)
	found (calc.)							
H ₂ L	74.1 (73.1)	5.0 (4.7)	5.2 (5.0)	11.1 (11.5)	279.36	280 [P] ⁺	Yellow (95%)	-
[Co(HL) ₂].H ₂ O, 1	64.1 (64.4)	3.6 (3.8)	4.4 (4.4)	11.4 (10.1)	633.63	631 [P-3H] ⁺	Dark green (55%)	3.32
[Cu(HL) ₂], 2	64.9 (65.8)	3.2 (3.9)	3.8 (4.5)	10.0 (10.3)	620.23	621[P] ⁺	Dark green (78%)	3.2
[Zn(HL) ₂], 3	65.1 (65.6)	3.9 (3.9)	4.3 (4.5)	10.4 (10.3)	622.09	623 [P] ⁺	Red (73%)	6
[Cd(HL) ₂], 4	59.9 (61.0)	4.6 (3.6)	3.9 (4.2)	10.2 (9.6)	669.09	670 [P] ⁺	Red (67%)	3.2
[Hg(HL)Cl], 5	39.5 (39.7)	2.4 (2.4)	2.6 (2.7)	6.8 (6.2)	514.43	515 [P] ⁺	Orange (90%)	14.9

Table 2

Compound	IR data							
	$\nu(\text{OH})$	$\nu(\text{NH}^+)$	$\nu(\text{C}=\text{N})$	$\nu(\text{C}-\text{O})$	$\nu(\text{C}-\text{S})$	$\nu(\text{M}-\text{O})$	$\nu(\text{M}-\text{N})$	$\nu(\text{M}-\text{S})$
H ₂ L	-	3262	1622(s)	1267(m)	708(m)	--	--	--
Complex 1	3463(b)	-	1602(s)	1213(m)	720(m)	504(w)	469(w)	427(w)
Complex 2	3455(m)	-	1603(s)	1215(m)	719(m)	505(w)	456(w)	407(w)
Complex 3	3440(m)	-	1616(s)	1216(m)	688(m)	498(w)	455(w)	415(w)
Complex 4	3420(m)	-	1613(s)	1209(m)	685(m)	487(w)	450(w)	410(w)
Complex 5	3410(m)	-	1615(s)	1214(m)	679(m)	504(w)	453(w)	412(w)

s, strong; m, medium; w, weak; b, broad; sh, shoulder.

Table 3

Compound	Chemical shift, δ (ppm)
H ₂ L	10.54 (s, 1H, OH), 8.44(s, 1H, HC=N), 7.00(s, 1H, SH), 7.82-6.61 (m, Ar-H)
Complex 3	9.45 (s, 2H, OH), 8.27 (s, 2H, HC=N), 7.76-6.91 (m, Ar-H)
Complex 4	9.27 (s, 2H, OH), 8.16 (s, 2H, HC=N), 8.13-6.83 (m, Ar-H)
Complex 5	9.50 (s, 1H, OH), 8.40(s, 1H, HC=N), 7.89-6.83 (m, Ar-H)

s, singlet; m, multiplet.

Table 4

Complex	Molecular formula	M.wt	Decomposition temperature(°C)	Weight loss%	Mass loss		Eliminated species	Solid residue (%)
					Calc.	Found		Found (cal.)
1	CoC ₃₄ H ₂₄ N ₂ O ₂ S ₂ (H ₂ O)	633.63	92-190	2.63	18.00	16.66	H ₂ O	Co
			206-548	59.56	376.42	377.39	C ₂₄ H ₁₂ N ₂ SO	9.43 (9.3)
			548-879	28.38	180.27	179.82	C ₁₀ H ₁₂ SO	
2	CuC ₃₄ H ₂₄ N ₂ O ₂ S ₂	620.23	200-387	30.87	192.26	191.46	C ₁₅ H ₁₂	CuO + 3C
			389-512	9.67	60.08	59.98	C ₂ H ₈ N ₂	19.63 (18.63)
			514-968	39.83	252.31	247.04	C ₁₄ H ₄ S ₂ O	
3	ZnC ₃₄ H ₂₄ N ₂ O ₂ S ₂	622.09	150-387	15.68	93.12	97.56	C ₆ H ₉ N	ZnO+8C
			388-528	30.69	192.15	190.85	C ₉ H ₆ NS ₂	28.73 (28.52)
			528-999	24.47	157.11	152.23	C ₁₁ H ₉ O	
4	CdC ₃₄ H ₂₄ N ₂ O ₂ S ₂	669.09	150- 378	58.05	387.41	388.41	C ₂₉ H ₁₁ N ₂	
			379-578	25.33	169.28	169.84	C ₅ H ₁₃ S ₂ O ₂	No residue
			578-999	16.62	112.41	111.20	Cd	
5	HgC ₁₇ H ₁₂ NOSCl	514.43	150-261	35.89	182.22	184.62	C ₁₃ H ₁₀ O	
			261-858	63.88	332.21	328.62	C ₄ H ₂ NSCl+Hg	No residue

Table 5

Complexes	Decomposition range (°C)	E*/Kjmol⁻¹	A*/s⁻¹	S*/Kjmol⁻¹	H*/Kjmol⁻¹	G*/Kjmol⁻¹
1	100-232	218.34	1.95	-243.43	17.79	135.86
	233-330	91.09	4.25x107	-104.08	864.96	144.43
	331-376	116.92	1.82x109	-73.91	111.66	158.37
	377-500	44.36	152.47	-210.18	38.58	184.45
2	257-361	113.39	7.06x108	-81.18	108.49	156.31
	456-763	7.11	0.027	-283.26	0.463	226.79
3	54-240	30.18	41.39	-218.29	26.02	135.16
	420-531	200.12	8.48x1012	-5.40	193.63	197.84
4	150-243	116.25	2x1011	-32.78	112.12	128.38
	244-334	75.91	16.57x105	-131.09	71.26	144.54
	490-576	54.37	373.23	-204.081	47.58	214.11
5	100-269	75.60	2.15x106	-128.429	71.21	139.03
	271-358	95.77	7.96x107	-98.99	91.06	147.09

Table 6

Compound	Bacterial strains				Fungal strains	
	<i>B. subtilis</i>	<i>S. aureus</i>	<i>E. coli</i>	<i>K. pneumoniae</i>	<i>C. albicans</i>	<i>A. niger</i>
Streptomycin	32.66 ± 0.33	45.33 ± 0.63	30.68 ± 0.22	28.53 ± 0.17	–	–
Nystatin	-	-	-	-	24.73 ± 0.57	29.53 ± 0.33
H ₂ L	10.60 ± 0.23	13.87 ± 0.28	7.67 ± 0.25	5.53 ± 0.24	4.87 ± 0.22	6.67 ± 0.16
Complex 1	18.73 ± 0.19	23.27 ± 0.55	15.67 ± 0.33	13.73 ± 0.10	12.00 ± 0.04	16.00 ± 0.27
Complex 2	24.27 ± 0.30	32.24 ± 0.18	20.87 ± 0.30	18.67 ± 0.69	16.67 ± 0.84	20.53 ± 0.66
Complex 3	13.53 ± 0.28	18.20 ± 0.14	11.33 ± 0.32	10.67 ± 0.34	8.33 ± 0.16	11.07 ± 0.50

The values are the mean of three experiments ± S.D.

Table 7

Compound	$K_b \times 104$ (M^{-1})	% Hypochromism	Red shift (nm)
H ₂ L	0.722	4.615	1
Complex 1	2.685	19.105	6
Complex 2	3.078	22.153	9
Complex 3	1.999	14.285	4

Table 8

Parameter	Complex 1	Complex 2	Complex 3	Complex 4
M-N32	1.942	1.974	2.113	2.464
M-S39	2.449	2.972	2.440	2.605
M-O19	2.181	2.068	2.216	2.485
M-O40	2.193	2.027	2.014	2.461
M-N52	1.938	1.992	2.146	2.437
M-S59	2.409	2.779	4.188	2.714
N32-C31	1.316	1.338	1.319	1.312
O40-C28	1.399	1.309	1.343	1.385
N52-C11	1.325	1.337	1.305	1.311
S59-C54	1.794	1.857	1.842	1.826
N32-C33	1.445	1.430	1.433	1.436
N52-C53	1.435	1.426	1.452	1.433
O19-C5	1.402	1.319	1.398	1.393
S39-C37	1.814	1.858	1.826	1.824
C31-C27	1.460	1.424	1.445	1.463
C27-C28	1.402	1.446	1.432	1.408
C11-C10	1.462	1.425	1.467	1.465
C10-C5	1.406	1.443	1.402	1.403
<N32MS39	88.441	77.114	85.338	76.950
<N32MO40	85.874	90.129	87.803	70.265
<O40MS59	92.436	87.879	45.954	70.662
<S59MN52	86.550	80.402	46.784	74.918
<N52MO19	87.341	86.296	79.249	68.266
<O19MS39	78.839	74.341	100.583	83.296
<N32C31C27	128.855	129.229	127.790	129.386
<N52C11C10	128.502	127.692	127.552	127.168
<S59C54C53	120.270	120.502	122.001	123.109
<O40C28C27	118.386	123.422	124.141	119.897
<O19C5C10	120.761	123.216	118.854	118.133
<MO40C28C27	35.579	19.086	-0.481	33.639
<MN32C31C27	-8.192	-11.649	-10.979	-13.876
<MS39C37C33	5.807	17.584	21.443	30.233
<MO19C5C10	-29.023	-26.987	-31.887	-50.715
<MN52C53C54	25.667	17.878	93.843	27.176
<MS59C54C53	15.170	-13.196	-30.872	-24.741
<MO40C28C29	-146.289	-162.509	-179.795	-147.327
<MN52C11H18	-172.599	-158.173	-173.925	-164.795
<MN32C31H47	171.598	169.831	166.969	164.166

Table 9

Parameter		Bond length		Bond angles		Dihedral angles	
ET, au	-852.761	M-O19	2.512	<S27MN20	77.330	<Cl33MO19H34	-3.889
E _{HOMO} , au	-0.2109	M-N20	2.562	<N20MO19	68.089	<Cl33MS27C22	-147.627
E _{LUMO} , au	-0.1003	M-S27	2.554	<O19MCl33	71.123	<S27C22C21N20	3.808
E _g , eV	3.010	M-Cl33	2.575	<Cl33MS27	148.997	<MS27C22C21	-29.594
I, eV	5.7364	S27-C22	1.834	<S27C22C21	124.251	<Cl33MN20C11	-48.239
A, eV	2.7281	C22-C21	1.426	<C22C21N20	120.314	<MN20C11C10	19.990
χ , eV	4.2322	N20-C21	1.435	<MS27C22	95.370	<N20C11C10C5	-3.765
η , eV	1.5041	N20-C11	1.313	<MN20C11	132.571	<Cl33MO19C5	169.569
S, eV ⁻¹	0.3324	C10-C5	1.407	<MO19C5	143.514	<MO19C5C10	-5.196
V, eV	-4.2322	C5-O19	1.385	<C11C10C5	124.081	<O19C5C10C11	-4.350

Table 10

Complex	Atomic No.	Natural charge	Natural population				Natural configuration
			core	valence	Rydberg	Total	
1	32	0.3319	17.9929	8.6558	0.0194	26.6681	[core] 4S ^{0.15} 3d ^{4.32} 5p ^{0.31}
2	33	0.8508	17.9945	10.1450	0.0094	28.1491	[core] 4S ^{0.14} 3d ^{4.98} 4p ^{0.08} 5p ^{0.16}
3	31	1.2642	18.00	10.7263	0.0094	28.7357	[core] 4S ^{0.35} 3d ^{9.98} 4p ^{0.40} 5p ^{0.01}
4	20	1.2381	36.00	10.7497	0.0139	46.7619	[core] 5S ^{0.42} 4d ^{9.99} 5p ^{0.34} 6p ^{0.01}
5	32	1.0693	68.00	10.9209	0.0097	78.9306	[core] 6S ^{0.69} 5d ^{9.97} 6p ^{0.25} 7p ^{0.01}

Table 11

Atom	Complex 1	Complex 2	Complex 3	Complex 4
N12	-0.4532	-0.6054	-0.5842	-0.5631
S19	-0.1212	0.0507	-0.0905	-0.3683
O63	-0.7524	-0.7392	-0.7494	-0.7766
N43	-0.4331	-0.6107	-0.6482	-0.5642
S50	-0.1647	-0.2050	-0.3814	-0.4060
O51	-0.6858	-0.6954	-0.8402	-0.7465

Table 12

Parameters	Complex 1	Complex 2	Complex 3	Complex 4
Effective core	30.0	30.0	38.0	56.0
Core	83.9575/84	83.9596/84	75.9652/76	75.9650/76
Valence Lewis	202.3369/203	204.3369/205	196.4822/206	196.2676/206
Total Lewis	306.5233/317	308.6061/319	310.4475/320	328.2327/338
Valence non-Lewis	10.8053/317	14.834/319	8.9939/320	9.1965/338
Rydberg non-Lewis	0.5711/317	0.5597/319	0.5585/320	0.5707/338
Total non-Lewis	10.4765/317	10.3937/319	9.5525/320	9.7672/338

Table 13

Parameter	Complex 1	Complex 2	Complex 3	Complex 4
ET, au	-1735.1675	-1786.19585	-1655.6912	-1638.1458
E _{HOMO} , au	-0.16265	-0.1964	-0.1794	-0.1864
E _{LUMO} , au	-0.09425	-0.1101	-0.1006	-0.0913
E _g , eV	1.861	2.349	2.145	2.590
I, eV	4.4227	5.3421	4.8796	5.0701
A, eV	2.5649	2.9947	2.7363	2.4833
χ , eV	3.4938	4.1684	3.8079	3.7767
η , eV	0.9289	1.7370	1.0716	1.2934
S, eV ⁻¹	0.5382	0.4260	0.4665	0.3865
V, eV	-3.4938	-4.1684	-3.8079	-3.7767

Table 14

Property	Urea	Complex 1	Complex 2	Complex 3	Complex 4	Complex 5
μ_x , D		1.8007	0.1987	3.5257	-2.1289	7.9967
μ_y , D		-7.6291	0.2371	-4.1905	7.7857	3.1439
μ_z , D		-3.9444	1.0163	-6.6554	-6.6602	-0.6512
μ , D	1.3197	8.7752	1.0623	8.6189	10.4678	8.6171
α_{xx} , au		23.7895	-228.0354	-226.1847	-227.4920	-135.6492
α_{xy} , a.u.		-2.1020	-9.9887	0.7454	2.2514	-12.4537
α_{yy} , a.u.		-246.1232	-235.7760	-256.7171	-248.8831	-146.2675
α_{zz} , a.u.		-248.0138	-240.4739	-230.1917	-257.1689	-161.8380
α_{yz} , a.u.		-7.1483	-8.0985	2.0184	17.0793	-7.7529
α_{xz} , a.a.		7.8863	2.7941	1.9726	-0.5738	0.7998
$\langle \alpha \rangle$, esu		-23.2351 $\times 10^{-24}$	-34.7916 $\times 10^{-24}$	-35.2268 $\times 10^{-24}$	-36.2370 $\times 10^{-24}$	-21.9214 $\times 10^{-24}$
$\Delta \alpha$, esu		40.1418 $\times 10^{-24}$	1.6122 $\times 10^{-24}$	4.2591 $\times 10^{-24}$	3.9307 $\times 10^{-24}$	3.3811 $\times 10^{-24}$
β_{xxx} , au		-47.3992	-23.5098	18.8544	-45.2534	-81.5257
β_{xxy} , au		-112.1607	-30.2299	-84.8500	-69.5818	-35.3583
β_{xyy} , au		-29.2390	-25.7844	30.3817	15.4326	-24.8850
β_{yyy} , au		-71.6153	71.3282	-15.8939	70.0172	-69.7986
β_{xxz} , au		-29.0839	-48.9994	-51.2057	-51.1718	5.2358
β_{xyz} , au		62.3177	-30.1936	-98.6022	-59.0234	19.7702
β_{yyz} , au		-11.3784	-46.1689	-4.5868	-13.4504	-0.2033
β_{xzz} , au		57.9328	66.7333	62.8780	7.4371	-102.6254
β_{yzz} , au		43.3971	-23.3709	18.6626	37.5012	-60.6249
β_{zzz} , au		-16.8114	109.2456	-54.9414	-27.8531	5.4419
$\langle \beta \rangle$, esu	0.1947 $\times 10^{-30}$	1.3197 $\times 10^{-30}$	0.2486 $\times 10^{-30}$	1.5349 $\times 10^{-30}$	0.8849 $\times 10^{-30}$	2.3066 $\times 10^{-30}$